RZ 3968 (#ZUR1912-029) 11/12/2019
Electrical Engineering 4 pages

Research Report

Weyl Semi-Metal-Based High-Frequency Amplifiers

A. Toniato[1], B. Gotsmann[1], E. Lind[2], and C. B. Zota[1]

[1] IBM Research Zurich, Saumerstrasse 3, Ruschlikon, Switzerland

[2] Lund University, Box 118, Lund, Sweden

Weyl Semi-Metal-Based High-Frequency Amplifiers

A. Toniato[1], B. Gotsmann[1], E. Lind[2], and C. B. Zota[1]
[1] IBM Research Zurich, Saumerstrasse 3, Ruschlikon, Switzerland, email: zot@zurich.ibm.com
[2]Lund University, Box 118, Lund, Sweden

***Abstract*—**In this work, we propose and simulate a novel amplifier based on Weyl semi-metals, e.g. WP_2 and MoP_2. These topological materials have been shown to exhibit extremely large magnetoresistance at cryogenic conditions. In the proposed device, a gate current induces a local magnetic field which controls the resistivity of the Weyl semi-metal channel and the resulting output current. Simulations of the magnetic fields are performed to optimize the device design, as well as thermal modeling to determine self-heating effects. Device operation is simulated using an analytical 3D model of magnetic fields and resistivity, and a small-signal model. Results show that the proposed device can provide high gain (20-30 dB) with extremely low DC power dissipation (40 μW) and high transition frequencies. This type of device is promising to replace HEMTs in quantum computers, where the low power dissipation enables it to be integrated at lower cryostat temperature stages.

I. Introduction

Topological Weyl semi-metals (WSM) such as WP_2, $PdSn_4$ and MoP_2 have received significant research attention recently due to their many unusual properties, including topologically protected states, hydrodynamic electron transport and extremely large magnetoresistance [1]. In these materials, topological protection leads to the formation of linear band dispersion crossing near the Fermi level [2]. Experimental fingerprints of WSM include detection of unconventional magneto-transport properties, such as extremely high temperature-dependent magnetoresistance (MR). MR as high as 10^6 % at 10 T and 0.35 K has been reported for WP_2 [3]. The physical origin of this MR is not yet understood but is suspected to be related to the underlying Weyl energy structure [4].

However, while WSMs provide rich opportunities for new physics, there is a lack of novel device concepts taking advantage of their unique transport properties. In this work, we propose and simulate an amplifier that utilizes the magnetoresistance of WSMs to provide high gain with low power dissipation. The amplifier consists of a metal conductor (gate) placed in close proximity to a WSM (channel). A current is passed through the gate which generates a local magnetic field modulating the resistivity of the WSM (**Fig. 1**). The very large MR coupled with the high free carrier concentration of the Weyl semi-metal allows for substantially higher transconductance as compared with semiconductor devices. Our modeling indicates that both current and voltage gain can be achieved at very low voltages, allowing for unique device operation surpassing that of semiconductor devices such as HEMTs. This type of device is highly attractive for qubit readout signal amplification in a quantum computer (i.e. in a cryostat, where cooling power is limited) and may represent a key area of application for Weyl semi-metals. Presently, HEMTs are used at the 4 K cryostat stage due to their high power dissipation, leading to reduced signal-to-noise ratio and high thermal noise, affecting the qubit coherence time and quantum gate speed. The proposed Weyl amplifiers can instead be placed directly at the 10 mK stage together with the qubits.

II. Device Operation and Modeling

Fig. 2 shows a schematic figure of the proposed WSM amplifier. The channel comprises a layer of WSM, such as WP_2, that is connected to source and drain metal electrodes, to which V_D is applied. The current I_D flows through the WSM. The channel is separated from the gate metal by an insulator, such as SiO_2. A gate bias V_G is applied at the gate terminal, which drives a gate current I_G. While the gate metal is in our simulations a superconductor, e.g. Nb (the WSM is not superconducting), that is not a necessary condition. I_G generates a magnetic field, which controls the resistivity of the WSM, described empirically as:

$$\rho(T,B)=\rho_0(T)\left[1+\alpha(T)\left(\frac{B}{\rho_0(T)}\right)^{m(T)}\right] \quad (1)$$

where ρ_0 is the resistivity in the absence of a magnetic field, α and m are empirical temperature-dependent parameters describing the magnetoresistance (MR) effect (**Fig. 3**). MR is present below ~50 K. Experimentally reported values of α and m for WP_2 are shown in **Table 1** [5]-[7]. In this work, we use α = 100 (unit omitted for clarity), m = 1.8. and ρ_0 = 0.2 μΩcm, unless otherwise stated.

Fig. 4 shows a flowchart of the device simulation procedure. For the simulations, the following conditions must be satisfied: (A) All current densities (I_G, I_D) are below the critical values for the respective material (Nb, WP_2) to maintain superconductivity and avoid material breakdown. (B) Self-heating is below 0.5 K to approximate ρ (T, B) ≈ ρ (T_0, B), where T_0 is the working temperature. (C) The magnetic field in the gate metal is below the critical field, 0.2 T for Nb.

First, device dimensions are determined to ensure uniform magnetic field in the WSM in order to avoid parasitic current paths, which would degrade device performance. This design rule (**Table 2**) is determined through magnetic field simulations in COMSOL. In our simulations, the gate current density is assumed uniform, i.e. not confined to the London penetration depth (which would result in a higher magnetic field near the WSM at a given current density), thus our simulation represents a worst-case scenario. The MR depends on the direction of the magnetic field, as only the y-component (from source to drain, **Fig. 2**) contributes to eq. (1). **Fig. 5** shows the magnetic flux density for a cross-section of the device in the x-direction. The design rule achieves high field uniformity and up to 0.18 T in the WSM channel. The influence of the magnetic field generated by the device current through the WSM channel during typical operating conditions is shown in **Fig. 5** and is

low enough to not break superconductivity in the gate (condition C) and has negligible effect on the WSM resistivity.

We calculate device self-heating to avoid temperature-dependent changes to the MR parameters α, m and ρ_0 during operation. The 3D differential heat equation was solved with COMSOL Multiphysics

$$\begin{cases} -\mathrm{div}(\mathrm{k}\nabla T) = V_D^2/\rho L_G^2 & \text{on } \Omega \\ -k\nabla T/\partial\vec{n} = 0 & \text{on } \Gamma_N \end{cases}$$

as well as T = 1 on Γ_D, where Ω is the domain denoting the whole device, Γ_N is the portion of the boundary where a zero-flux boundary condition is imposed (consistent with a device operation in high vacuum) and Γ_D denotes the boundaries in direct contact with the heat sink, corresponding to T = 1 K. k is the thermal conductivity for the different materials (Nb, SiO_2, WP_2), $\vec{n}$ is the normal to the surface. In **Fig. 6** the self-heating for a device with L_g = 1.1 µm is reported. A drain voltage sweep was performed in order to define the $V_D \approx 3$ mV for which the self-heating would not surpass 0.5 K in 1 K ambient.

After establishing the required dimensions according to the design rule, the maximum current densities fulfilling condition A are determined. As the resistance of the superconducting gate is 0 Ω, R_G can be determined by an external resistor. It is set such that $J_G < J_C$ (conditions A and C) given that V_G is in the order of the target input voltage (~10 µV for qubit readout).

To determine the DC characteristics, the channel (WSM) is modeled as a 3D resistor network (shown for two dimensions in **Fig. 7**). Each resistor element is calculated numerically using eq. (1) and the point-wise simulated y-component of the generated magnetic field:

$$B(\vec{r}) = \frac{\mu_0}{4\pi}\int_V \frac{J_G(\vec{r}') \times (\vec{r} - \vec{r}')}{|\vec{r} - \vec{r}'|^3}\,\mathrm{d}\vec{r}'$$

where $J_G = V_G/R_G$ is the gate current density, $\vec{r}$ indicates a point in the channel (a resistor network element), and $\vec{r}'$ is the position of an infinitesimal magnetic-field source in the volume V of the gate metal. Finally, DC characteristics are determined by the resistor network and the V_D from the thermal model.

III. Performance

The transfer characteristics of the WSM amplifier is shown in **Fig. 8**. The current is normalized to the cross-sectional area of the WSM, as well as the gate metal width. Note that the different gate lengths shown result in completely different device geometries, as well as R_G and V_D, according to the design rule in **Table 2**. The maximum current density at L_G = 22 µm is 45 mA/µm². The transconductance, g_m, is shown in **Fig. 9** versus V_{GS} normalized to the gate metal width. The WSM can achieve very high g_m > 5000 mS/µm. The transconductance is $g_m = \partial I_D/\partial V_{gs} \cong V_D(L_g)/\Delta R_{WSM}(L_G)\,\Delta V_{gs}$. The L_G-dependence of V_D is determined by the simulations of self-heating, such that for a given L_G, V_D is set to the value corresponding to a maximum of 0.5 K temperature increase (~1-5 mV). This dependence is non-linear and relates to the boundary conditions of the heat transfer model. The increase of g_m for longer L_G, up to 22 µm, is due to in part this effect, in part the increased WSM height, H_C, that can maintain a uniform magnetic field. The output conductance, g_d, is relatively independent of device dimensions while following the design rule (**Fig. 10**). The voltage gain, g_m/g_d, is thus primarily dependent on g_m and reaches a maximum of 8 at L_G = 22 µm (**Fig. 11**). The effect of α on g_m is shown in **Fig. 12** for different reported experimental values. **Fig. 13** shows the influence of the oxide thickness t_{ox} on L_G = 22 and 1.1 µm devices. t_{ox} will mostly impact DC performance when it is approximately thicker than the WSM channel (H_C = 550 and 27.5 nm, respectively). Scaled t_{ox} does not result in significantly higher g_m since the gate metal height is $L_G/2 >> t_{ox}$ and the magnetic field is uniform at below 0.2 T. For RF operation, $t_{ox} \approx H_C$ is ideal, in order to reduce the gate capacitance. Normalized DC power dissipation, P_{DC}, is shown in **Fig. 14** versus L_G.

The small signal model (**Fig. 15**) is derived as a hybrid-π model approximated from a physical large-signal model. Similar to HBTs, the (kinetic) inductance due to the gate current is considered negligible at <300 GHz. Also, no frequency-dependence of MR is assumed. The resulting Y-parameters are also shown. High-frequency gain is shown in **Fig. 16** for an RF-optimized design (t_{ox} = 100 nm) with I_{DS} = 10 mA. The gate capacitance is calculated as $\varepsilon W_M \times L_M/t_{ox}$. We focus on C-band operation (where inductive effects can be neglected), as in a quantum computer. A power gain of 26 dB can be achieved at 5 GHz, with a P_{DC}, of 40 µW, driving 10 mA of output current. As opposed to in an FET, the gate capacitance is in the Weyl amplifier not used to modulate the channel resistance, resulting in very low RC delay and large bandwidth, though inductive effects must be considered above 300 GHz. A comparison with commercial cryogenic (multi-stage) HEMTs is shown in **Table 3** at both 5 GHz and 80 GHz (at identical I_{DS}), the latter being a potential future quantum computer operation frequency. The proposed device achieves similar gain levels with up to 250x lower P_{DC}. This low P_{DC} crucially enables integration close to the qubit in a quantum computer cryostat (10 mK stage), where cooling power is limited to <100 µW, resulting in increased signal-to-noise ratio due to the lower thermal noise.

Future work towards realizing this promising device concept includes epitaxial growth of WSMs to enable standard fabrication techniques and determining the size and frequency-dependent material properties.

IV. Conclusions

We have proposed and simulated the DC and RF characteristics of a novel amplifier based on the magneto-transport properties of Weyl semi-metals. Based on experimentally demonstrated material parameters, the proposed amplifier achieves a gain of 26 dB at 5 GHz with a very low power dissipation of 40 µW, comparing favorably with commercial cryogenic HEMTs. The promising performance of the proposed amplifier shows the strong potential of Weyl semi-metals in electron devices.

References

[1] A. A. Soluyanov et al., *Nature*, vol. 527, pp. 495, 2015.
[2] M.-Y. Yao et al., *Phys. Rev. Lett.*, vol. 122, p. 176402, 2019.
[3] R. Schonemann et al., *Phys. Rev. B*, vol. 96, p. 121108, 2017.
[4] N. Kumar et al., *Nat. Comm.*, vol. 8, p. 1642, 2017.
[5] R. Schonemann et al., *Phys. Rev. B*, vol. 96, p. 121108, 2017.
[6] A. Wang et al., *Phys. Rev. B*, vol. 96, p. 121107, 2017.
[7] J. Du et al., *Phys. Rev. B*, vol. 97, p. 245101, 2018.

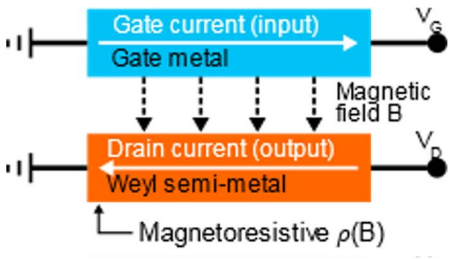

Fig. 1. Schematic figure of the basic operation of the proposed Weyl semi-metal (WSM) amplifier. The channel comprises a gate metal and a WSM channel. An input gate bias drives a gate current that generates a local magnetic field. The magnetic field modulates the resistivity of the WSM through its magnetoresistance, amplifying the input signal at the drain output.

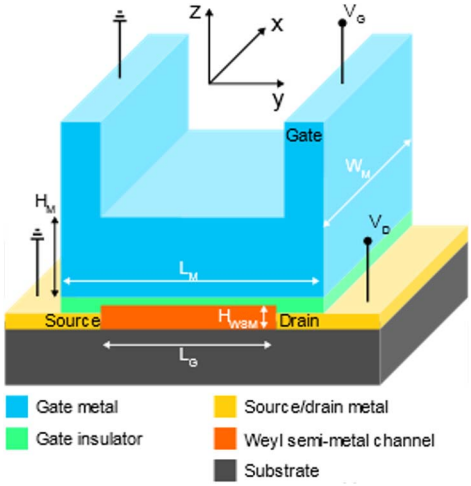

Fig. 2. Schematic of the simulated device structure. Note that the width of the WSM, W_C, is not shown for clarity. As shown in Table 2, it is half of W_M.

Ref	β	α	ρ_0 (μΩcm)
A. Wang	2.5	1.8	0.19
Schonemann	1150	1.8	0.01
J. Du	96	1.8	0.03

Table 1. Experimentally determined material parameter values for WP_2 at below 5 K. The large discrepancy in α and resistivity can be attributed to different growth conditions and methods.

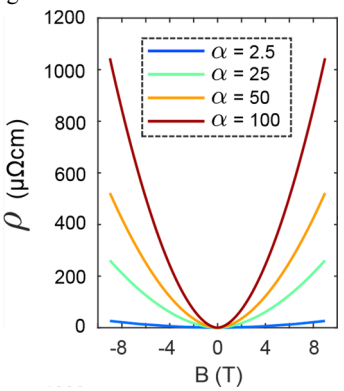

Fig. 3. Magnetoresistance effect in Weyl semi-metals at temperatures below ~50 K, showing increased resistivity at high magnetic fields.

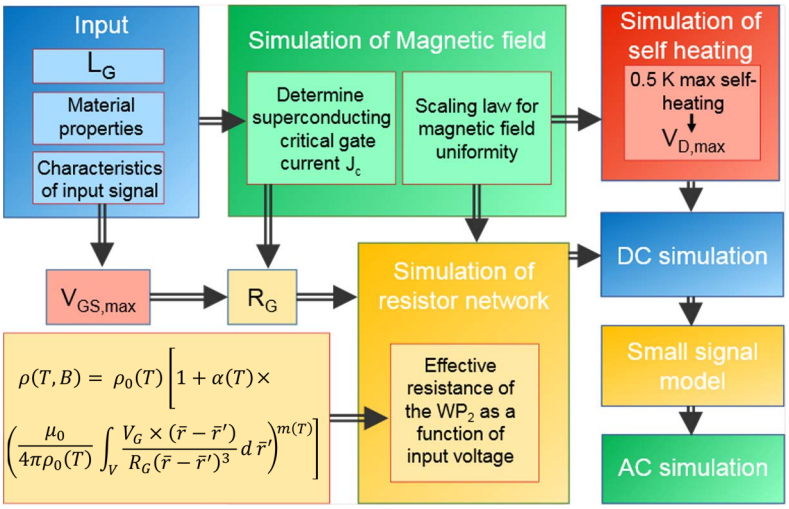

Fig. 4. Flowchart for the Weyl amplifier simulation procedure. Input parameters are gate length, Weyl material properties (Table 1) and target input signal voltage (~10-20 μV). 3D magnetic field simulations in COMSOL determine a design rule that produces a uniform magnetic field below the critical field strength. R_G is tuned to give a gate current below the critical current of the gate metal, as the gate metal itself has 0 Ω (i.e. R_G is used to transfer the input gate bias to a current). Self-heating simulations determine maximum $V_{D,max}$ that keeps self-heating below 0.5 K. DC properties are calculated analytically using a resistor network and $V_{D,max}$. A small-signal is derived to determine RF properties.

Parameter	Design factor
Gate metal length L_M	2k
Gate width W_M	k
Gate height H_M	k/2
Channel length L_G	**k**
Channel width W_C	k/2
Channel height H_C	k/40
Oxide thickness t_{ox}	100 nm
Zero-field resistivity ρ_0	0.2 μΩcm

Table 2. Design rule to maintain uniform magnetic field in the Weyl semi-metal.

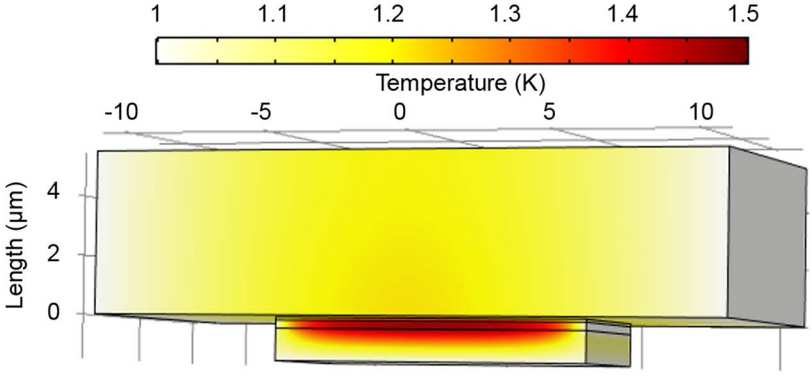

Fig. 6. Self-heating simulations in COMSOL, at an ambient temperature of 1 K. The drain voltage is swept until self-heating is 0.5 K. This maximum drain voltage (typically in the order of mV) is subsequently used to determine the DC properties of the amplifier.

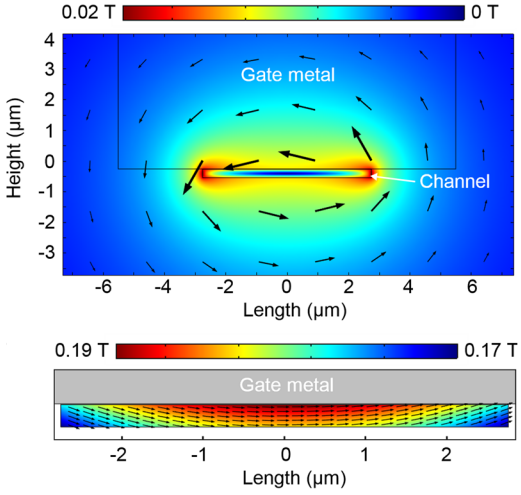

Fig. 5. Magnetic field simulations in COMSOL Multiphysics in the x-direction (Fig 2.). Top shows field by the WSM and bottom by the gate. We establish a design rule (Table 2) that maintains uniform magnetic field below the critical field of 0.2 T.

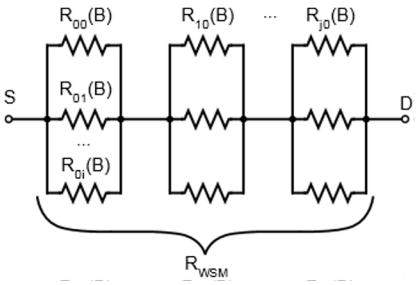

Fig. 7. The Weyl semi-metal channel is modeled as a 3D resistor network as shown above (for only 2 dimensions). Note that vertical resistor elements are omitted due to the layered (2D) nature of the WSM.

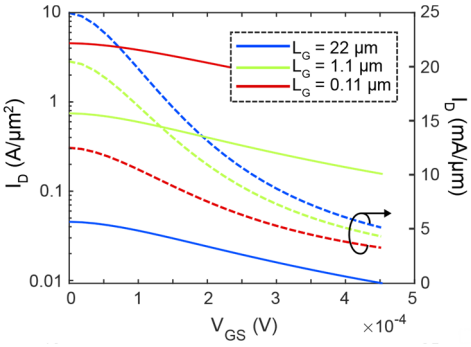

Fig. 8. Transfer characteristics of simulated Weyl amplifiers with various device dimensions. Note that while only L_G is indicated, other dimensions vary according to the design rule in Table 2. Left-hand axis is normalized to channel cross-section, and right-hand axis to gate width.

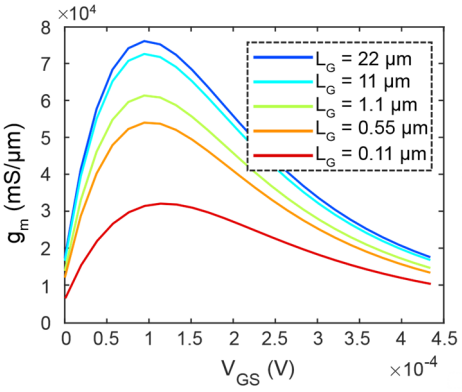

Fig. 9. Transconductance (normalized to gate width) for different device geometries. The reduction of g_m at short L_G is due to the decreased channel height and the increased self-heating, leading to lower V_D.

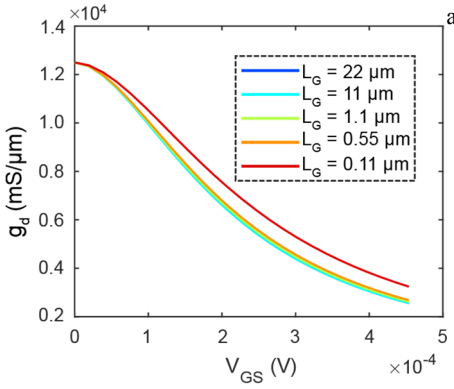

Fig. 10. Output conductance $g_d = dI_D/dV_D$ for different device geometries.

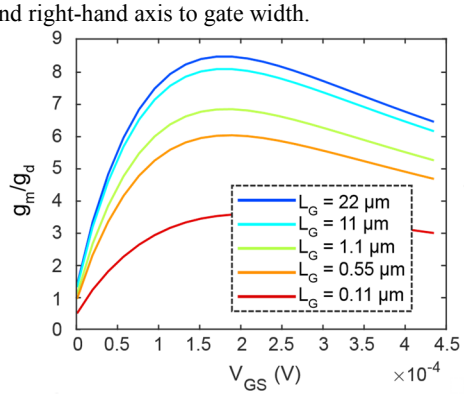

Fig. 11. Voltage gain for different device geometries. The voltage gain is primarily dependent on g_m.

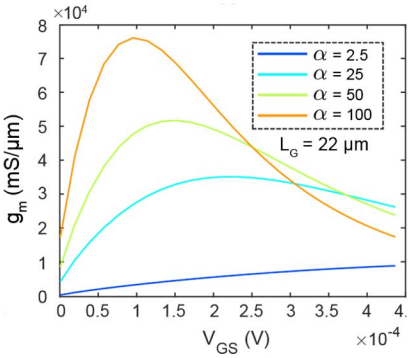

Fig. 12. Transconductance for devices with L_G = 22 μm and different values of the magnetoresistance parameter α, which describes the strength of the modulation of resistivity at a given magnetic field.

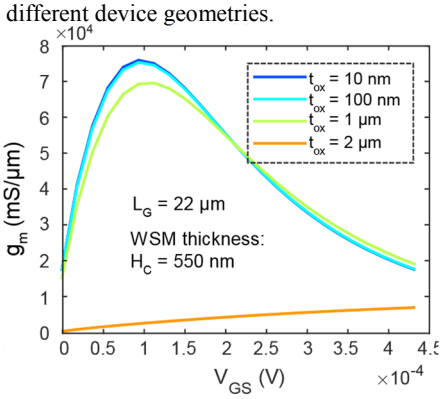

Fig. 13. The gate oxide impacts performance when it is thicker than the channel, H_C.

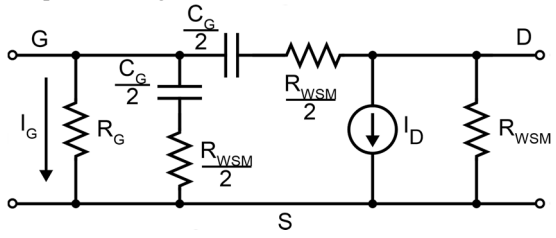

Fig. 16. Hybrid-π small signal model for the proposed device. This model is valid up to about 300 GHz, where inductances can be neglected. The derived y-parameters are shown to the right.

$$y_{11} = \frac{1}{R_G} + 2y_g \qquad y_g = \frac{j\omega C}{1+j\omega RC}$$
$$y_{21} = g_m - y_g \qquad C = \frac{C_G}{2}$$
$$y_{12} = -y_g \qquad R = \frac{R_{WSM}}{2}$$
$$y_{22} = \frac{1}{R_{WSM}} + y_g$$

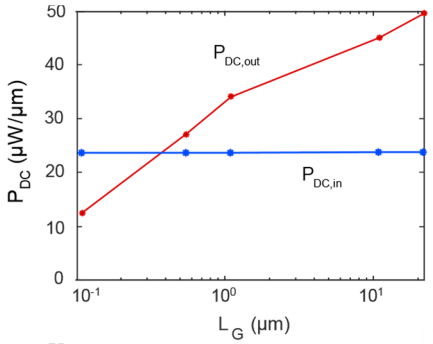

Fig. 15. DC power consumption normalized to gate width and versus device dimensions. The higher $P_{DC,out}$ at longer L_G is due to higher I_{DS} as shown in Fig. 8.

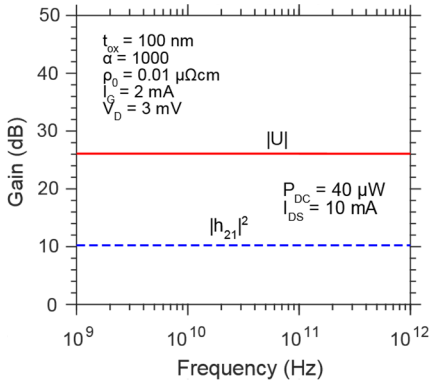

Fig. 17. Gain plot of a simulated Weyl amplifier with design optimized for RF, based on the small-signal model. Due to the low intrinsic RC delay, the cut-off and maximum oscillation frequencies are very high.

Parameter	Cryo HEMT*	Weyl Amplifier
Gain (5 GHz)	39 dB	26 dB
P_{DC} (5 GHz)	7 mW	44 μW
I_{DS} (5 GHz)	11 mA	11 mA
Gain (80 GHz)	25 dB	26 dB
P_{DC} (80 GHz)	7 mW	28 μW
IDS (80 GHz)	7 mA	7 mA
Cryostat stage†	4 K	10 mK

*Low Noise Factory (LNC4_8 & LNC65_115).
†Indicates lowest cryostat stage with sufficient cooling power.

Table 3. Comparison between the proposed device and commercial cryogenic HEMTs. The Weyl amplifier is biased at the same I_{DS} as the HEMT.

ACKNOWLEDGEMENTS
This project has received funding from the European Union's Horizon 2020 research and innovation programme under grant agreement No 829044 (SCHINES).